By Catherine J. Murphy*
Department of Chemistry and Biochemistry
University of South Carolina
Columbia, South Carolina 29208

and

Jeffery L. Coffer
Department of Chemistry
Texas Christian University
Fort Worth, Texas 76129

Quantum Dots: A Primer

INTRODUCTION

Crystalline inorganic solids can be divided electronically into three well-known classes: metals, semiconductors, and insulators. In these extended solids, atomic orbitals overlap to give nearly continuous electronic energy levels known as bands.[1] Metals are electronically characterized by having a partially filled band; semiconductors have a filled band (the valence band) separated from the (mostly) empty conduction band by a bandgap E_g, corresponding to the familiar HOMO-LUMO energy gap for small molecules. Insulators are conceptually the same as semiconductors in their electronic structure, except that the bandgap is larger in insulators (Fig. 1). In terms of E_gs, metals have E_g less than ~0.1 eV; semiconductors have E_gs from ~0.5 to ~3.5 eV; and insulators have E_g > ~4 eV. (1 eV = 1.602×10^{-19} J = 8065.5 cm^{-1}).

There are some key differences, however, between the electronic structure of molecules and solid-state materials such as semiconductors. The description of an electron moving through a solid lattice is generally derived as a modification of a free electron wave upon encountering point charges that represent the atoms. In the free-electron model, the electron's momentum is proportional to k, the "wave vector" which is related to its wavelength λ:[1]

$$k = 2\pi/\lambda \qquad (1)$$

In solving the Schrodinger equation for an electron in terms of its wavelength (and hence k), one finds that the energy levels, in the one-dimensional case, are

$$E = h^2k^2/(8\pi^2m) \qquad (2)$$

where E is the energy of the electron, m is its mass, and k is its wave vector.[1]

The simplified band structure diagram of Fig. 1 can be redrawn in terms of k (Fig. 2). Note that from Eq. 2, the shape of the energy bands is parabolic with respect to k. Semiconductors in which the lowest-energy transition does not involve a change in k are called "direct bandgap" materials; conversely, semiconductors in which the lowest-energy transition does involve a change in k are "indirect bandgap" materials. Electronic transitions for which $\Delta k \neq 0$ are formally forbidden, although defects in the lattice and other reductions in symmetry may make the transitions more allowed.[1,9]

Silicon and germanium in Group IV are the only two elements that are semiconductors. Si and Ge are both indirect bandgap materials. Compound semiconductors "average" out to these electron configurations in general; thus GaN, GaP, GaAs, InP, and InAs are III–V semiconductors, while ZnO, ZnS, CdS, CdSe, and CdTe are II–VI semiconductors. Several other oxides also exhibit semiconductive behavior (TiO_2, WO_3). Periodic trends in semiconductive behavior are observable; for example, E_g decreases as one moves down a column in the periodic table. The more ionic semiconductors tend to be direct bandgap materials and thus are more suitable for light-emitting applications.

If the particle size of a bulk inorganic crystalline solid is on the order of nanometers, it is now well-known that interesting optical and electronic effects may result. Semiconductors with all three dimensions in the ~1–10 nm size range are referred to as "quantum dots;" in this size range,

* Author to whom correspondence should be sent.

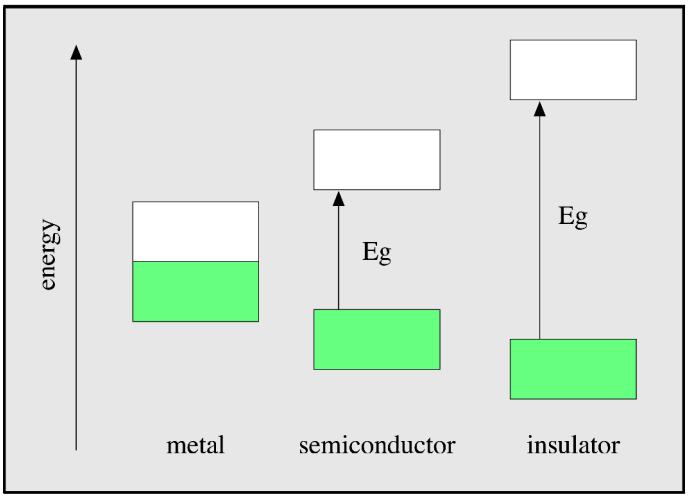

FIG. 1. A simplified energy level diagram for metals, semiconductors, and insulators. The shaded boxes represent the filled valence bands; the empty boxes represent the empty (at 0 K) conduction bands. The arrows represent the bandgap energy E_g.

electrons exhibit quantum mechanical effects.[2–10] In the literature, semiconductor quantum dots are also known as semiconductor nanocrystals or nanoparticles.

Consider what happens when a semiconductor is irradiated with light of energy $h\nu > E_g$. (For semiconductors, this corresponds to light in the near IR, through the visible, and extending into the ultraviolet region). An electron will be promoted from the valence band to the conduction band, leaving a positively charged ''hole'' behind. This hole can be thought of as the absence of an electron and acts as a particle with its own effective mass and charge in the solid. One can calculate the spatial separation of the electron and its hole (an ''exciton'') using a modified Bohr model:

$$r = \epsilon h^2/\pi m_r e^2 \qquad (3)$$

where r is the radius of the sphere defined by the three-dimensional separation of the electron-hole pair; ϵ is the dielectric constant of the semiconductor; m_r is the reduced mass of the electron–hole pair; h is Planck's constant; and e is the charge on the electron. For many semiconductors, the masses of the electron and hole have been determined by ion cyclotron resonance[1,9] and are generally in the range of 0.1 m_e to 3 m_e. For typical semiconductor dielectric constants, the calculation suggests that the electron–hole pair spatial separation is ~1–10 nm for most semiconductors.[9] In this size range, when the exciton is created, the physical dimensions of the particle confine the exciton in a manner similar to the particle-in-a-box problem of physical chemistry. Therefore, the quantum effects such as quantization of energy levels can be observed in principle. Alternatively, one can think of the nanoparticle as having an electronic structure intermediate between bands and bonds (Fig. 3). One consequence of this intermediate character is that E_g is correlated with size: as the dimensions of the particle decrease, E_g increases.

Brus has developed a popular effective mass model that relates particle size (neglecting spatial correlation effects) to the bandgap energy of a semiconductor quantum dot:[12]

$$E_g(\text{quantum dot}) = E_g(\text{bulk}) + (h^2/8R^2)(1/m_e + 1/m_h) - 1.8e^2/4\pi\epsilon_0\epsilon R \qquad (4)$$

where E_g is the bandgap energy of the quantum dot or bulk solid, R is the quantum dot radius, m_e is the effective mass of the electron in the solid, m_h is the effective mass of the hole in the solid, and ϵ is the dielectric constant of the solid. The middle term on the right-hand side of the equation is a particle-in-a-box-like term for the exciton, while the third term on the right-hand side of the equation represents the electron–hole pair Coulombic attraction, mediated by the solid. Implicit in this equation is that the quantum dots are spherical and that the effective masses of charge carriers and the dielectric constant of the solid are constant as a function of size. The Brus model maps E_g and size well for larger quantum dots, but its predictions do not match experiment well for very small particle sizes. Many other more complex approximations have been derived theoretically that better match experimentally determined

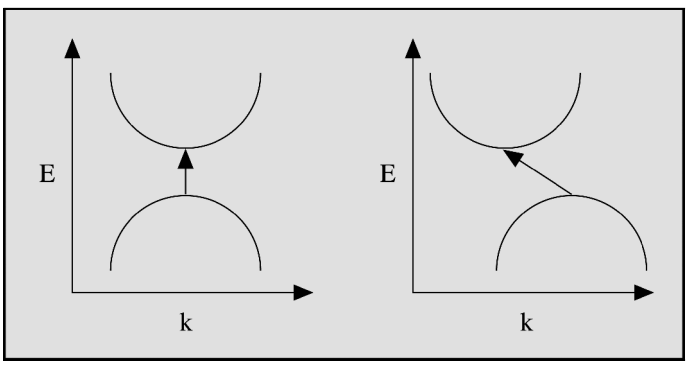

FIG. 2. Electronic band structure of direct (left) and indirect (right) semiconductors. The arrows show the lowest-energy transition between the valence band (bottom curves) and conduction band (top curves); a change in k is necessary for the indirect semiconductor.

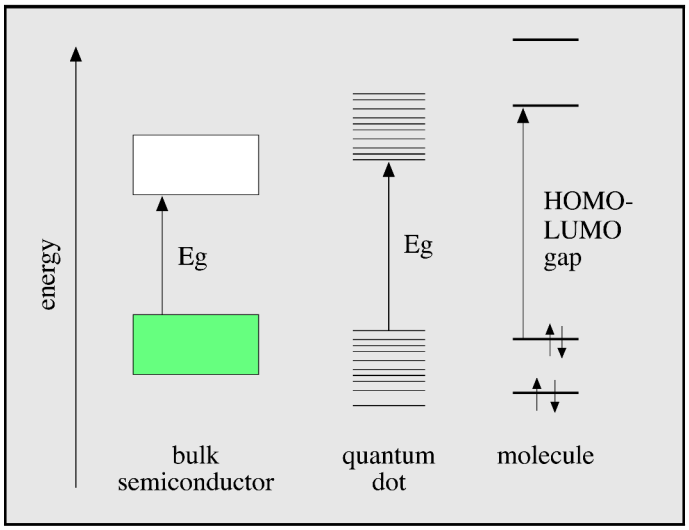

FIG. 3. Energy level diagram comparing a bulk semiconductor to its molecular analog (e.g., bulk Si compared to Si clusters of a few atoms) and a quantum dot. The semiconductor's electrons are in bands; the molecule's electrons are in molecular orbitals (bonds). The vertical arrow denotes the bandgap E_g for the bulk semiconductor, and the highest occupied molecular orbital-lowest unoccupied molecular orbital (HOMO-LUMO) energy gap in the molecule. On the nanometer scale, the electronic structure of a semiconductor quantum dot is in the intermediate regime between bands and bonds.

bandgap energies and quantum dot sizes.[5–9] Many excellent reviews of the electronic and optical properties of quantum dots are available.[2–10] In particular, some workers refer to quantum dots as ''artificial atoms'' because their quantized electronic states bear many analogies to atomic electronic states.

SYNTHESIS

As quantum dots are not (yet) commercially available, the spectroscopist must either make these nanomaterials in the lab or collaborate with a synthetic chemist. Thus, a substantial portion of this article examines the current methods of making these materials.

There are two general approaches to synthesizing quantum dots. One of these is the ''bottom-up'' approach, more familiar to chemists: molecular or ionic precursors to the quantum dots are allowed to react together in solution to produce the quantum dot materials as colloids. The other approach, more familiar to engineers, is the ''top-down'' approach: feature sizes on the 1–10 nm scale are carved out lithographically or electrochemically from a semiconductor substrate. Hybrid approaches are also possible; for example, chemists make molecular precursors for the quantum dots, which then react in the gas phase and are deposited as thin films on substrates.

Synthesis From the Bottom Up: II–VI Materials. CdS and CdSe have been the most well-studied of these materials, due to the availability of precursors and ease of crystallization, and also due to their bandgap energies. In the bulk, at room temperature, the E_g of CdS is 2.4 eV (~520 nm); E_g for CdSe is 1.7 eV (~720 nm). Thus, quantum dots made of these materials will have E_gs in the visible and just into the ultraviolet range; the corresponding onset of absorption can be readily monitored with standard spectrophotometers (see below).

Arrested Precipitation. From the Ksp of CdS, it is clear that simply mixing Cd^{2+} and S^{2-} solutions in water (at nanomolar concentrations or higher) would lead to the precipitation of CdS. One method of arresting this precipitation is to mix aqueous solutions of Cd^{2+} first with a water-soluble polymer that has basic coordinating groups, such as polyphosphate[12] or amines.[13,14] The subsequent addition of sulfide results in the formation of CdS quantum dots whose size depends on the relative concentration of reagents, pH, temperature, etc. The function of the polymer in this case is to compete with sulfide for metal ion binding sites and, presumably, to sterically hinder small nanoparticles from aggregating together and growing into larger ones.

Organometallic Precursors. The most highly cited method for making CdE (E = S, Se, Te) quantum dots is that of Murray, Norris, and Bawendi.[15] In this synthesis, $Cd(CH_3)_2$ is mixed with a chalcogenide reagent in a coordinating solvent (trioctylphosphine oxide; this also acts as a surfactant) at relatively high temperature (200–350 °C) in an inert atmosphere. Careful control of monomer injection rates, temperature, concentration, etc., leads to crystalline nanoparticles coated with surfactant that are highly monodisperse compared to other methods (5% standard deviation in diameter from the average). A recent report suggests that CdO, far less toxic than dimethylcadmium, can be used as the Cd precursor to CdE quantum dots with the chalcogenides as elements in a phosphonic acid solvent/surfactant.[16] Well-defined molecules containing both the Group II element and the Group VI element as a single-source precursor can be decomposed to produce II–VI quantum dots.[17,18]

Particle Growth Termination with a Capping Agent. Thiols under basic solution conditions can be deprotonated to thiolates, RS^-, that compete very well with sulfide ligand(s) in making CdS or ZnS quantum dots. Again, final particle size is dictated by solution conditions, most importantly the ratio of sulfide to thiolate.[19–23] The final CdS or ZnS nanoparticles, then, are capped with thiolates:

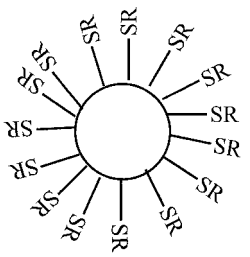

Synthesis Inside a Nanoscale Cavity. If the reaction between divalent cadmium or zinc with sulfide or selenide is performed in a restricted environment on the nanometer scale, then II–VI quantum dots will be formed. Examples of nanoscale cavities include porous glasses and xerogels,[24] reverse micelles,[25] zeolites,[26] membranes,[27] Langmuir–Blodgett films,[28] and hollow proteins.[29]

Biosynthesis. Yeast and tomatoes, and likely other organisms, produce CdS quantum dots as a detoxification response to an overload of cadmium;[30,31] the CdS thus produced is coated with particular peptides, which in turn can be used as the stabilizing thiol to make CdS quantum dots as described above.[32]

Synthesis From the Bottom Up: III–V Materials. The direct gap character for many III–V compound semiconductors, coupled with their associated luminescence behavior in real devices,[33] makes the construction of three-dimensionally confined nanocrystals of this family of semiconductors an important goal. At the same time, challenges associated with achieving crystallinity in III–V materials of nanophase dimension add an extreme level of synthetic complexity to such studies.

Core/Shell Nanocrystals. Synthetically, the pioneering use of dehalosilylation reactions by Wells and co-workers has proven to be a useful route for the formation of a wide variety of nanocrystalline III–V materials,[34] the early paradigm being GaAs.[35,36] While the size-dependent spectroscopic behavior of a number of III–V species (such as InP[37]) have been thoroughly investigated, the metastability of surface-capping moieties for many III–V nanocrystals interferes with the radiative recombination of electron–hole pairs by the introduction of detrimental interfacial defects. Hence, very recent independent approaches by Nozik et al.[38] and Banin and co-workers[39] involving the formation of hybrid core/shell nanocrystal systems are of value in this regard. As pointed out by these groups, in the design of such core/shell structures, it is important for the core and shell interfaces to be lattice-matched (Fig. 4). If this is not the case, strain develops during growth, relieved only by the formation of large numbers of interfacial defects on the core surface; incomplete cap growth is also likely. Capping a quantum dot core with a larger-bandgap semiconductor shell has also been used to stabilize the core in II–VI materials.

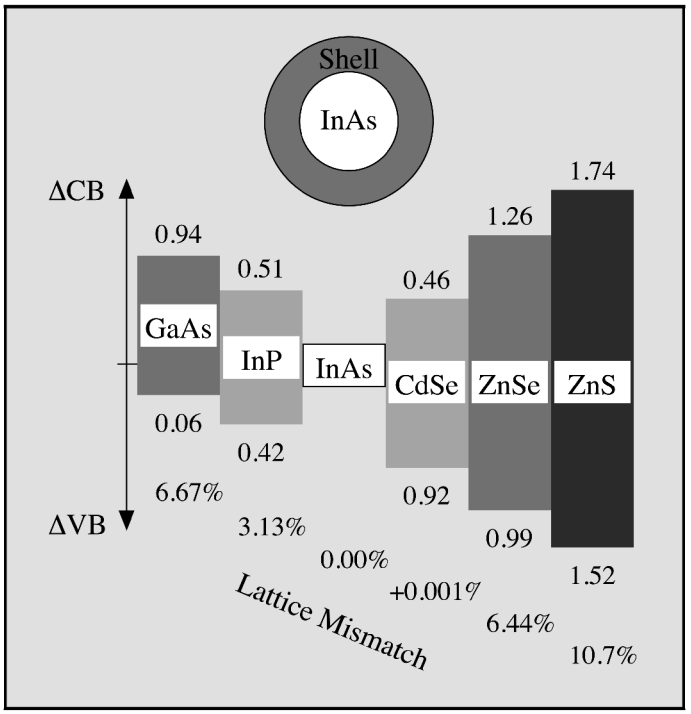

FIG. 4. Band offsets (eV) and lattice mismatch (%) in core/shell nanocrystals based on an InAs core and various shell structures (adapted from Ref. 39).

The approach of Banin and co-workers has entailed the synthesis of a number of shell structures (InP, GaAs, CdSe, ZnSe, and ZnS) on InAs cores in a two-step process.[39] By monitoring core/shell growth with absorption and photoluminescence spectroscopy, it is found that the bandgap of the core shifts to the red upon growth of InP or CdSe shells, while for the larger bandgap shells, ZnSe and ZnS, the band gap energy of the core is maintained. It is important to note that the photoluminescence quantum yield is quenched in InAs/InP core/shells, but increases up to 20% for InAs/CdSe and InAs/ZnSe core/shell nanocrystals. For InAs/ZnS core/shell materials, the enhancement of the photoluminescence quantum yield is apparently smaller (~8%).

The work of Nozik and co-workers has focused on the use of Zn-$CdSe_2$ capping layers on InP nanocrystals, known to provide strain-free interfaces in the bulk.[38] The lattice matching permits epitaxial growth of the $ZnCdSe_2$ shell on colloidal InP nanocrystals; shell thicknesses up to 50 Å were grown on the InP nanocrystal core. The $ZnCdSe_2$ shell causes a shift of the electronic states of the core–shell nanocrystals to lower energy compared to pure InP quantum dots. For small core sizes, the electron is apparently delocalized over the whole nanocrys-

tal, while the hole is mainly localized within the core region. Theoretical calculations have been employed to determine the electron probability density of the quantum dots and compared with the experimental results.

Group III Nitrides. One class of III–V nanocrystalline materials receiving extensive recent interest is the nitrides, especially GaN. Such materials are of interest given the possibility of blue emitting lasers, light-emitting diodes (LEDs), and robust photodetectors based on this semiconductor.[40,41] Routes to nanocrystalline gallium nitride have been reported that permit some control over the particle size and a degree of crystalline phase-inhomogeneity of the materials. One viable precursor is polymeric gallium imide, $\{Ga(NH)_{3/2}\}_n$, which can be converted to nanocrystalline, cubic/hexagonal GaN.[42] Another method involves routes to gallazane, $[H_2GaNH_2]_x$, from the combination of $LiGaH_4$ and NH_4X (X = Cl, Br) in Et_2O.[43]

Synthesis From the Bottom Up: Group IV Materials. Much, but not all, of the interest concerning the preparation of nanocrystalline elemental semiconductors from this Group has focused on the paradigm of solid-state microelectronics: silicon. Common bottom-up routes for the preparation of homogeneous Si nanocrystals include the gas-phase pyrolysis of silane or disilane,[44–47] as well as the Zintl phase route of Kauzlarich and co-workers using NaSi in a glyme-type solvent under inert conditions.[48]

Advances in Group IV nanocrystal synthesis have not been limited exclusively to silicon. The Zintl phase route noted above has also been successfully extended to germanium[49–51] and tin.[52] For the case of Ge, these nanocrystals can be prepared via the reaction of NaGe (or KGe or MgGe) with excess $GeCl_4$ in glyme-type solvents at reflux temperatures. Depending on solvent and surface termination, crystalline Ge nanocrystals ranging in size from 4.5 to 10 nm can be obtained, with a relatively broad size distribution. While inhomogeneously broadened, there is clearly a size-dependent shift in the emission maxima of these samples. Ge nanocrystals with a mean diameter of 3.5 nm emit clearly in the blue, 6.2-nm particles in the yellow-green, and 8–10-nm crystallites in the red. For Sn, the nano-sized particles are prepared by the reaction of $SnCl_4$ with Mg_2Sn in glyme. Interestingly, Sn core structures with Si shells can also be constructed by substituting $SiCl_4$ for the tin halide species in the above reaction. High resolution transmission electron microscopy (HRTEM) analyses confirm that crystalline Sn in a tetragonal structure is obtained; solid state NMR spectra and X-ray powder diffraction confirm the β-tin environment.[52] Typical nanoparticle diameters for these materials range from 7 to 15 nm.

Capping Si quantum dots with SiO_2 is difficult to avoid, but is beneficial in that it protects the underlying Si from further oxidation. One of the intrinsic difficulties associated with oxide-capped Si nanocrystals is the difficulty in achieving monodisperse size distributions, notably accentuated by the aggregation tendency of the SiO_2 capping layer. Hence viable surface modification routes are an important part of advances in this area, ideally to ease both purification and processing in other requirements. This is also a strength of the Zintl approach noted above, whereby the as-prepared nanoparticle surfaces are reactive (given their chlorine termination) with alkyl lithium reagents such as methyl or butyl lithium or Grignard reactants such as octylmagnesium bromide.[53] Such transformations permit alkyl-functionalized surfaces with ample solubility in organic solvents. For the case of erbium-doped silicon nanocrystals, the Coffer group has also encountered success with the use of surface derivatization reactions employing functional groups with slightly different polarities, i.e., $-SiMe_3$, $-Si(CH_2)_3CN$, and $-Si(CH_2)_3NH_2$; such surface modification occurs most effectively when the capping agent is present as the nanoparticles are collected in the bubbler immediately after their formation in the pyrolysis oven.[54] While the derivatized, doped nanocrystals retain the desired luminescence at 1540 nm, associated with the erbium centers, for the $-SiMe_3$ and $-Si(CH_2)_3CN$-capped nanocrystals there is a clear improvement of their solubility in solvents such as butylphenyl ether. In contrast, propylamine-modfied surfaces become less soluble in the solvents tested, presumably as a consequence of extensive hydrogen bonding induced aggregation. In general, the ability to work with these nanocrystals in a wider variety of solvents may not only improve size-selective quantum dot isolation but also their use in other applications.

Synthesis From the Top Down. Lithographically patterned quantum dots, painstakingly fabricated from a series of plasma or wet chemical etched processes and anchored to a substrate, remain the method of choice for much of the solid-state physics and engineering communities.[33] However, the focus of this part of the review is an examination of relatively facile methods, almost all electrochemical in nature, for producing quantum dots of a given type by self-limiting reactions. Based on ties to industrially relevant wet etch processes, such reactions have typically focused on semiconductors from the Group IV family.

The paradigm of this type of material is porous silicon: porous layers of nanocrystalline Si wires and dots typically prepared by a constant current anodization of bulk crystalline Si in ethanolic HF. While its existence has been known since 1956,[55] interest in porous Si experienced something of a renaissance in the 1990s as a consequence of Canham's discovery of visible light emission from porous Si in 1990.[56] A number of developments have been described by Buriak in a recent review.[57]

As with quantum dots prepared from bottom-up approaches, these top-down electrochemical routes are not restricted simply to silicon. A

very recent account by Buriak and Choi has described a novel biopolar etch process for the fabrication of porous germanium.[58] Using HCl as an etchant, a brief (5 min) anodic etch at relatively high current densities (~350 mA/cm^2) produces a surface chloride and/or hydroxide layer that subsequently dissolves; a switch to cathodic bias of the same magnitude for one minute is believed to be a crucial step for the formation of a hydride-terminated porous Ge surface. A four electron reduction of a given Ge center in an acidic environment is proposed:

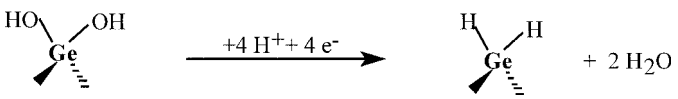

In contrast to porous Si, only extremely weak red emission is detected at 77 K by the unaided eye from these bipolar-etched porous Ge structures (with 365-nm excitation), a luminescence that is apparently too weak to be observed with charge-coupled device (CCD) detection.[58] The anodically etched layers, on the other hand, produce yellow-white photoluminescence upon excitation with 254-nm light at 77 K. The latter emission is believed to be oxide related, given the absence of Ge–H_x species in these films and the fact that their brief exposure to a 25% aqueous HF solution eliminates this type of luminescence. Thus, it is proposed that the weak emission emanating from the bipolar-etched, hydride-terminated material originates from Ge nanoparticles, while that of the anodically etched oxide structures is a consequence of oxide.[58]

OPTICAL, ELECTRONIC, AND STRUCTURAL CHARACTERIZATION

For colloidal solutions of quantum dots, electronic absorption spectroscopy is a simple and easy way to estimate the bandgap energy. Figure 5 illustrates the UV-vis spectra for CdS nanoparticles with diameters of ~2–10 nm; as the nanoparticle decreases in size, the band edge blue-shifts. For a semiconductor that has a bulk bandgap in the near-IR, its visible color can be tuned from black (bulk) to red, to yellow, to white, depending on nanoparticle size.[4]

Photoluminescence in quantum dots arises from the radiative recombination of electron–hole pairs (Fig. 6). The fate of the photogenerated electron–hole pair in the solid is critically tied to applications of these materials. Slight defects in the solid, such as vacancies, impurities, or adsorbates at the surface cause the formation of ''trap'' states into which the photo-excited electron can fall, or the photo-excited hole can ''float.''

The resulting photoluminescence can thus be quite Stokes-shifted from the absorbance, depending on the relative energies of these trap states compared to the valence and conduction band edges. The photo-excited electron or hole can interact with adsorbates in a donor–acceptor charge-transfer manner familiar to inorganic chemists[59] to yield changes in emission lifetime or quantum yield, forming the basis for some sensor applications. If the electron–hole pair does not recombine in the solid, it may reduce or oxidize molecules at the surface (e.g., TiO_2 photocatalysis). One way to eliminate trap states is to coat the quantum dot with a shell of a higher-bandgap material; this leads to light emission that is quite close to the absorption energy and that can have quantum yields approaching 0.50.[60–62] Thus, emission spectra are also often obtained for quantum dot materials as a means to characterize them.

Due to the sensitivity of photoluminescence of quantum dots to defects and adsorbates, the optical properties of the materials may depend heavily on the synthetic procedure used to make them. For example, in the pyrolysis of organometallic precursors to make GaN quantum dots, generally intrinsic bandgap photoluminescence (emitting in the blue region with a maximum near 410 nm) and/or broad defect photoluminescence (known to emit in the yellow region) can be observed.[63] In general, the observed emission spectra are strongly dependent on pyrolysis temperature and choice of precursor. GaN derived from pyrolysis of a solid gallium imide precursor typically exhibits yellow defect photoluminescence, with the reaction temperature influencing the intensity of the emission. Pyrolysis of this same precursor in a relatively high boiling amine solvent yields blue photoluminescence with an emission maximum near 420 nm. GaN derived from pyrolysis of a polymerized gallazane precursor, in contrast, yields blue light emission whose quantum yield can be improved by a brief HF etch, presumably through the reduction of nonradiative pathways. The core-shell synthetic approaches outlined above can be beneficial in reducing defect emission and promoting band-edge electron–hole recombination.

Emission spectra for quantum dots can be extremely narrow[5–10,62] (Fig. 7). Quantum yields as high as 0.5 have been reported.[60,62] Time-resolved photoluminescence data are complex and depend a great deal on sample quality; time scales from femtoseconds to microseconds have been observed and correlated with electron trapping times (femtoseconds to picoseconds), band-edge electron–hole pair recombination (picoseconds to nanoseconds), and electron–hole pair recombination from trap states (nanoseconds to microseconds); in addition, microsecond lifetimes are observed due to recombination from ''dark'' excitonic states at low temperature.[5–10,62,64]

Doping bulk semiconductors with part-per-million levels of impurities is a well-recognized means of con-

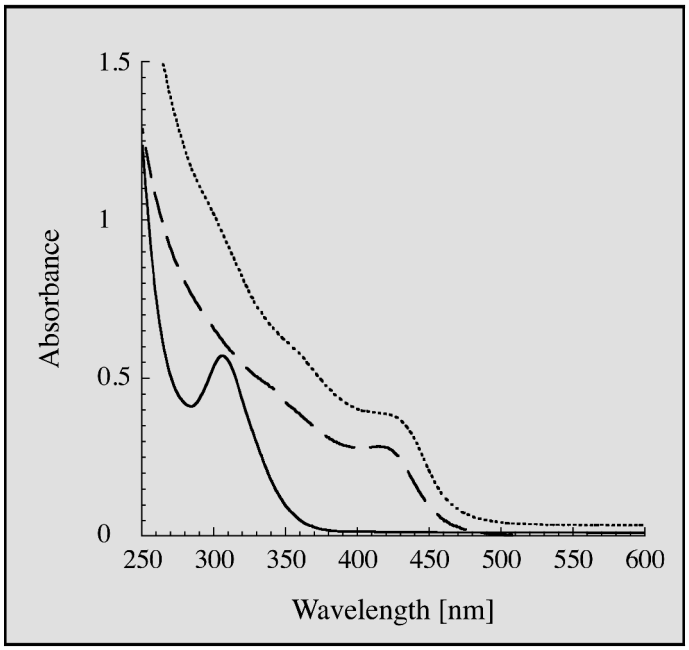

FIG. 5. Ultraviolet-visible absorption spectra of CdS quantum dots of different diameters in aqueous solution; 20 Å (solid line), 40 Å (dashed line), and 125 Å (dotted line).

trolling electronic and optical properties.[1,11] Quantum dots can be doped with metal ions that have energy states within the bandgap, and light emission from these introduced trap states can be observed.[64–72] For the case of Si nanocrystals, the Coffer group at Texas Christian University has recently succeeded in the preparation and characterization (both structural and photophysical) of discrete Si nanoparticles doped with Er^{3+} ions.[71,72] Erbium is of particular interest in this regard because of its known emission at 1540 nm, the transmission maximum of SiO_2. Such nanoparticles are prepared via a gas-phase pyrolysis of disilane in the presence of an erbium chemical vapor deposition (CVD) precursor and harvested as a colloidal solution in the reactor. Unlike other known homogeneous Si nanocrystals (and porous silicon), these Er^{3+} doped Si nanocrystals solely yield the desired near IR photoluminescence associated with the erbium centers as a result of carrier-mediated excitation from the Si exciton.

Electronic effects in quantum dots have been intensely explored by the condensed-matter physics community.[73,74] Only one quantum effect will be described here: the ''Coulomb blockade''.[75,76] [75,76]. Because of the small size and quantized nature of the electronic states within a quantum dot, adding a single electron to a quantum dot costs a great deal of energy, with additional electrons costing even more; thus, electron flow through a quantum dot can only proceed one electron at a time, creating the ''blockade''.[75,76] This blockade effect could in principle be used to construct nanoscale gates and cavities that could form the basis for new optical and electronic devices.

Characterization of Colloidal Quantum Dots. Quantum dot size is best measured by transmission electron microscopy (TEM). High-resolution TEM (HRTEM) can visualize lattice fringes, leading to crystallographic information about the particle, including its phase and crystal axes.

X-ray diffraction of dried-down colloidal nanoparticles can be used to infer particle size from the broadening of the diffraction peaks. Energy X-ray absorption fine structure (EXAFS) is also a valuable technique in providing details of coordination number and local geometry in semiconductor nanocrystals, particularly in very small dots where a large percentage of the total atom composition is present at the surface (with an accompanying amount of strain).[77] In direct gap systems, ab-

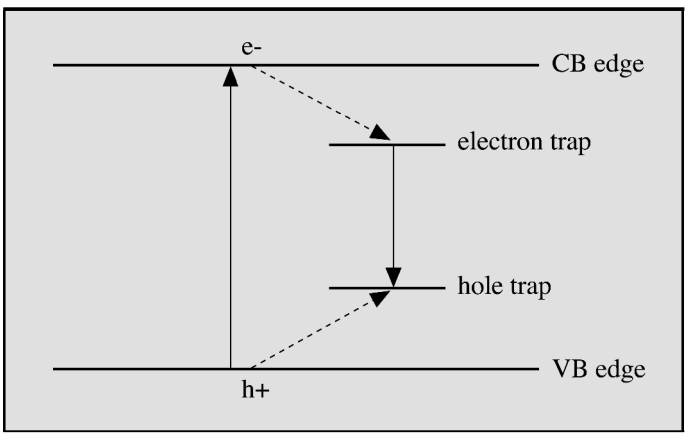

FIG. 6. Photoluminescence from a semiconductor quantum dot. Upon absorption of a photon, or electrical excitation (solid up arrow), an electron from the valence band is promoted to the conduction band, leaving a hole behind. If trap states are present in the bandgap (due to impurities, defects, etc.), the electron and hole can be trapped (dashed arrows). Photoluminescence (solid down arrow) results when the electron and hole recombine to emit a photon of light. For defect-free and impurity-free semiconductors, the luminescence is from radiative band-edge recombination. Not shown are nonradiative decay pathways for electron–hole recombination.

sorption spectroscopy is used extensively to evaluate E_g, which is correlated with nanoparticle size as well (see above). Standard chemical techniques, such as nuclear magnetic resonance (NMR), elemental analysis, etc., can be used to characterize the composition of the material.

Characterization of Supported Quantum Dots. In addition to optical spectroscopy, scanning electron microscopy (SEM), scanning probe microscopies (SPM), and HRTEM are critical means of evaluating quantum dots made from the ''top down.'' SEM is a very commonly employed method, and information concerning feature size is easily obtained in cross sectional analyses, as exemplified by Fig. 8, which contains an image of porous Ge.

APPLICATIONS OF QUANTUM DOTS FOR THE ANALYTICAL CHEMISTRY COMMUNITY

Applications of quantum dots can be classified as: (1) light sources, (2) photonics, (3) photovoltaics, and (4) photoluminescent dyes and sensors. The light source and photovoltaic applications require that the quantum dot be supported and electrically connected to other electronic elements in a device. Quantum yields of ~0.2 have been reported for simple solution-phase preparations of colloidal CdS,[13] and quantum yields of up to 0.50 are achievable with more elaborate preparations.[60,62] Light-emitting diodes based on quantum dots[78,79] and quantum cascade lasers based on quantum wells (two-dimensional semiconductor nanostructures) have been reported;[80,81] in theory, quantum dot cascade lasers are achievable.[82] In the quantum cascade laser, unlike semiconductor diode lasers, the wavelength output is dependent upon quantum confinement effects. Stimulated emission and optical gain from CdSe quantum dots have been reported.[83] In recent exciting work, semiconductor nanorods (cylinders, not spheres, on the nanometer scale) have been shown to exhibit polarized light emission and lasing.[107,108]

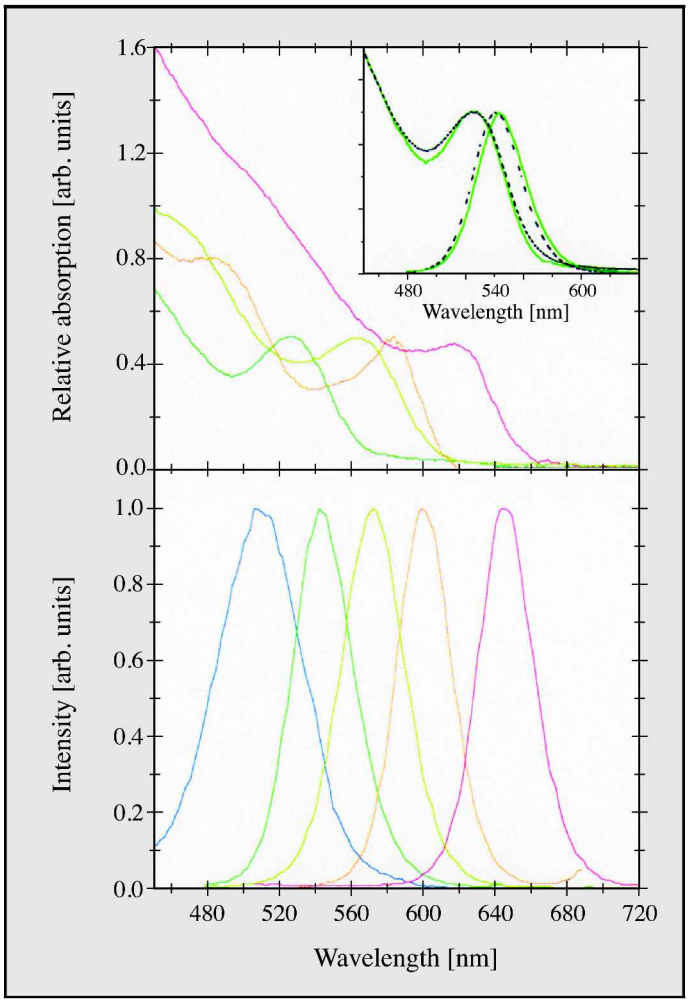

FIG. 7. Absorption (upper panel) and emission (lower panel) spectra of a series of CdSe quantum dots surface-stabilized with a shell of ZnS, and subsequently silanized for improved water solubility. The change in optical properties is a function of the size of the CdSe core, which is varied from 2.7 to 4.1 nm. The dots are dissolved in an aqueous buffer solution at pH ~7. The data are normalized for the convenience of the display. From left to right, blue, green, yellow, orange, and red emitting nanocrystals are shown. For blue emitting quantum dots, the absorption spectrum does not show features above 450 nm and is therefore omitted. Inset: Absorption and emission of silanized green-emitting nanocrystals in 10 mM phosphate buffer (solid lines), and of the same green CdSe/ZnS particles in toluene (dashed lines). Reprinted with permission from Ref. 99. Copyright 2001 American Chemical Society.

As noted earlier, the demonstration of efficient visible luminescence from nanocrystalline Si remnants present in porous Si roughly a decade ago[56] generated tremendous excitement with the prospect of legitimate Si based optoelectronics.[84] However, the heterogeneity of the nanostructures in this matrix and long-term stability issues pose serious hurdles to authentic device development.[85] Thanks to the recently reported results of Pavesi and coworkers, some of the problematic issues concerning light emission from nanocrystalline silicon have now been resolved in an elegant manner.[86] These workers have demonstrated optical gain from Si nanocrystals at room temperature, with net modal gain values on the order of 100 cm^{-1} reported.[86] A key step in securing

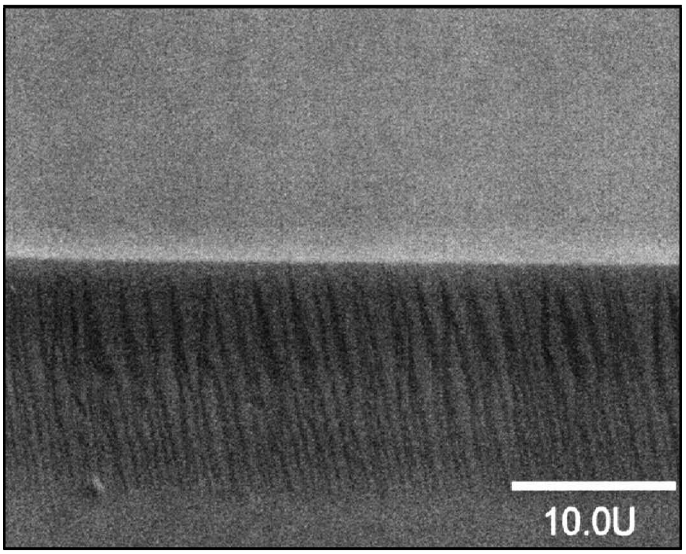

FIG. 8. Cross-sectional scanning electron micrograph of a porous Ge film. The columnar structure is clearly present. Scale bar = 10 μm (J. Buriak and H. Choi, Purdue University).

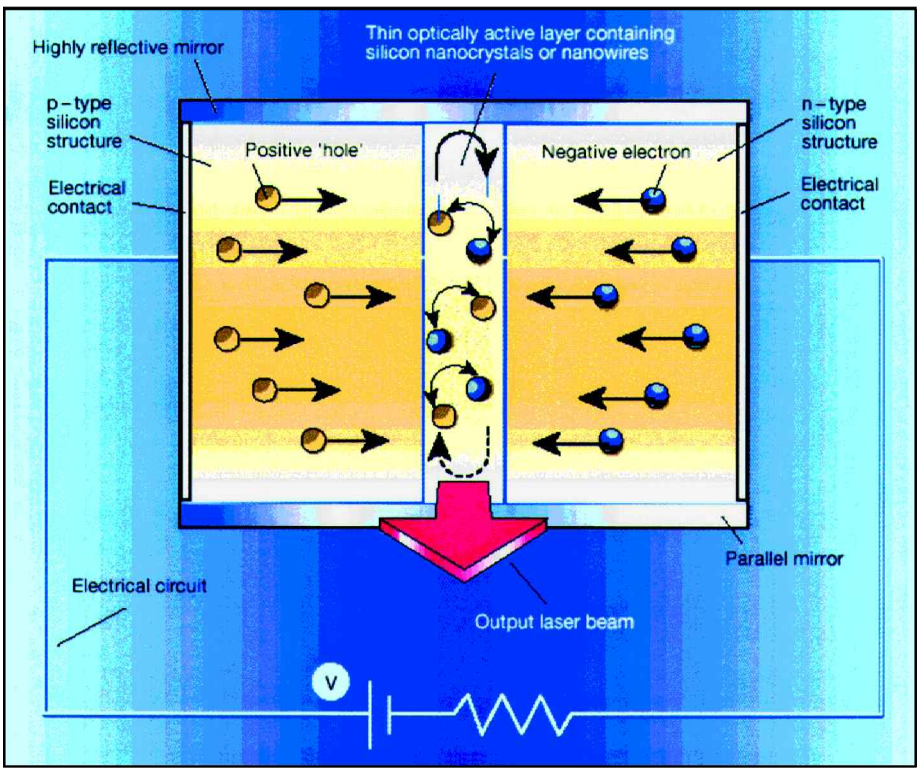

FIG. 9. Proposed operational scheme of a Si nanocrystal-based laser. Upon the application of voltage, p-type and n-type semiconductor layers donate positively charged 'holes' and negatively charged electrons, respectively, to the structure. Electron–hole recombination within the active region produces a photon and leads to the emission of light. With adequate efficiency of light emission that is located between two highly reflective mirrors, such an emitter can be turned into a miniature laser. (Adapted from Ref. 89).

this result was the use of ion implantation methods, in conjunction with careful thermal annealing, to produce closely packed arrays of Si nanocrystals (with relatively few defects) in a SiO_2 matrix. Pavesi and co-workers suggest that the ability to achieve gain in these nanocrystals is also strongly dependent on the quality of the Si/SiO_2 interface, with a relatively high number of emissive states per Si quantum dot. One very interesting and perhaps controversial manifestation of this interfacial quality is the presence of a unique absorption band in the near infrared, attributed to a Si=O species.[87,88] In any event, as pointed out by Canham,[89] demonstration of optical gain is a major step in the right direction toward fabrication of a Si based laser, but the production of coherent light from this type of structure remains to be shown. In this regard, however, key issues have been identified and a plausible scenario for such a device has been described (Fig. 9).[89]

While the Coffer group has noted a bottom-up approach to kinetically trapped erbium ions into discrete Si dots,[71,72] Fauchet and co-workers have exploited the large surface area-to-volume ratio of porous Si for facile Er^{3+} ion incorporation into this matrix and subsequently observed the desired near IR electroluminescence.[90] This is achieved by cathodic electrochemical migration, followed by a relatively high temperature anneal (950–1100 °C) in an oxygen or nitrogen ambient. The use of an extremely thin (~13 nm) semitransparent Au layer facilitated carrier injection into the active emitting region either through forward or reverse bias, with the resultant electroluminescence at 1.54 μm associated with the erbium centers clearly observed.[90] While the structures exhibit an exponential electroluminescence intensity dependence for either bias direction, differences in device characteristics as a function of temperature suggest that slightly different excitation mechanisms are operative. Upon increasing the operating temperature from 240 to 300 K, the luminescence intensity decreased by a

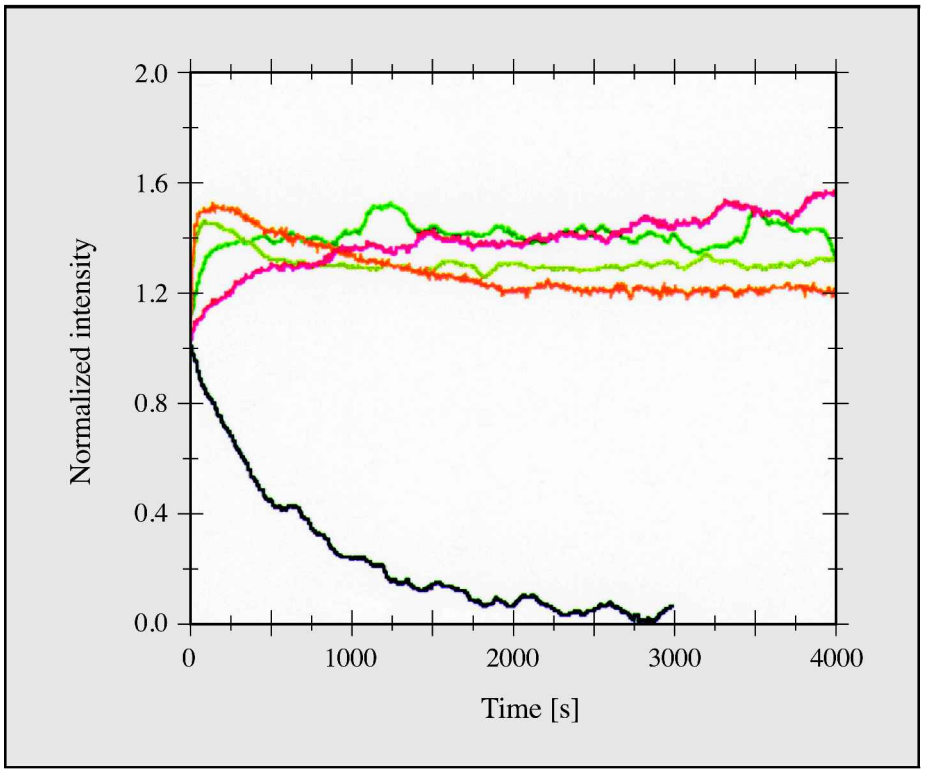

FIG. 10. Time dependence of the fluorescence intensity of CdSe quantum dots, capped with ZnS and silanized as in Fig. 7, compared to rhodamine 6G under continuous Ar^+ laser irradiation (0.5 mW; spot size, 700 μm; volume of sample, ~1 mL; absorbance = 0.065 at 488 nm). The quantum dots are stable for at least four hours, while the organic dye bleaches after ~10 min. The colored lines correspond to the emission color of the quantum dots; the black line is rhodamine 6G. Reprinted with permission from Ref. 99. Copyright 2001 American Chemical Society.

factor of 24 under reverse bias and only a factor of 2.6 under forward conditions. Such differences have been explained on the basis of a hot electron impact mechanism in reverse bias, where larger temperature quenching effects could arise as a result of inefficient transport through the Er doped porous Si matrix. While further studies are ongoing, it is encouraging to note that external quantum efficiencies on the order of 0.01% have been detected in these systems.

In a subsequent report, Lopez and Fauchet have successfully constructed one-dimensional photonic bandgap structures from a related yet slightly more complex device architecture.[91] A photonic bandgap material is one in which certain frequencies of light cannot be propagated in certain directions, just as the electronic bandgap in semiconductors does not permit certain energy levels.[92] In this specific system, highly reflecting porous silicon Bragg reflectors (each containing six pairs of low and high porosity layers) are fabricated, which sandwich an active layer; the cavities are doped with erbium by the cathodic electromigration process (as above) and activated by a high temperature anneal in oxygen and nitrogen. Interestingly, the position of the Er^{3+} emission maximum may be tuned in such structures by controlling the oxidation temperature. One assessment of the optical quality of such structures is the cavity quality factor Q, defined as the wavelength of the resonance divided by the full width at half-maximum intensity. Q values on the order of 130 have been reported for this emission, with corresponding full width at half-maximum intensity as narrow as 12 nm.

Photovoltaics—the conversion of sunlight to electricity—is another application in which quantum dots may provide some advantages. The ideal photovoltaic device would be one in which a significant portion of the solar spectrum would be absorbed, efficient charge separation would be achieved, and transport of charge through the device would be efficient. Quantum dot/polymer composite photovoltaic devices have been reported with internal conversion efficiencies of 2.7%, which are respectable compared to the best photovoltaics based on silicon (10%);[93] as the intricacies of the system are worked out, much higher efficiencies may be achievable.

Colloidal quantum dots with well-passivated surfaces (so that trap states are avoided in photoluminescence) can function as large ''fluorescent dyes'' that have narrow emission spectra (Fig. 7) and relatively high quantum yields.[94–99] CdSe in the bulk absorbs light from 720 nm into the ultraviolet; quantum dots of CdSe also absorb in the ultraviolet but cut off at different wavelengths depending on particle size[94–99] (Fig. 7). Covalent attachment of biological molecules to the quantum dot surface has been demonstrated, and these bioconjugates of quantum dots have been used to visualize receptor–ligand interactions in cells, as DNA hybridization probes, and for other biotechnological applications.[94–99] Compared to organic dyes, quantum dots have narrower emission spectra (~30 nm FWHM), and many different fluorescence colors can be excited with a single wavelength of light[100] due to the overlapping absorptions at the high-energy end of the electronic spectra (Fig. 7). The extinction coefficients of quantum dots have been reported to be on the order of ~100 000 M^{-1} cm^{-1}.[99] Since the emission lines are relatively narrow compared to organic dyes, detection of the quantum dots suffers much less from cross-talk that might result from the emission of a different fluorophore bleeding into the de-

tection channel for the fluorophore of interest. There is also evidence that quantum dots, suitably surface-derivatized for protection, are much more stable than organic fluorescent dyes (Fig. 10); one study reports that quantum dots are stable in solution for a month over a pH range of 6–8, and that under light irradiation, no photobleaching is observed for at least four hours (Fig. 10).

However, the surface chemistry of quantum dots still needs to be further worked out, and there have been reports of ''photobrightening'' (the opposite of photobleaching!), which are still not understood.[99]

For chemical sensor or biosensor applications, the quantum dot surface should not be passivated to the point where it is insensitive optically to its environment, but the surface should be available for interactions with analytes. This application of quantum dots is a broad frontier that is gaining increasing interest. The use of the photoluminescence of quantum dots for detection of different DNA sequences, based on the differential adsorption of DNAs to the quantum dot surface due to local DNA structural deformation, has been reported by the Murphy group.[101–106] Local structural and dynamic distortions within DNA are correlated with some genetic diseases, and thus, quantum dots, unique probes with curvature on the size scale of the distortion, may be well-suited as optical detectors of DNA deformation and damage.[109]

CONCLUSION

The 1990s saw incredible progress in the synthesis, characterization, and the beginnings of applications for quantum dots. Dramatic improvements in particle dispersity and quantum efficiency of emission have brought the notion of authentic devices based on these materials closer to fruition. However, there is still a great need for better synthetic methods for making these materials on a large scale, with less toxic precursors.

In the construction of real devices, hybrid materials entertaining mixtures of inorganic quantum dots with semiconducting organic architectures, will likely play a key role. The biological applications of quantum dots, unexpected in the early 1990s, are now a likely area for high impact and commercial potential in the near future.

ACKNOWLEDGMENTS

The authors thank their co-workers listed in the references. In addition, the authors thank the National Science Foundation (DMR 98-19178 to J.L.C., CHE 95-02929 to C.J.M.), the National Institutes of Health (C.J.M.), the Research Corporation (C.J.M. is a Cottrell Scholar), the Alfred P. Sloan Foundation (C.J.M.), the Camille and Henry Dreyfus Foundation (C.J.M.), and the Welch Foundation (J.L.C.) for financial support of their quantum dot work.

1. N. B. Hannay, in *Semiconductors,* N. B. Hannay, Ed. (Reinhold, New York, 1959).
2. M. L. Steigerwald and L. E. Brus, Acc. Chem. Res. **23,** 283 (1990).
3. H. Weller, Adv. Mater. (Weinheim, Ger.) **5,** 88 (1993).
4. H. Weller, Angew. Chem. Intl. Ed. Engl. **32,** 41 (1993).
5. A. P. Alivisatos, J. Phys. Chem. **100,** 13226 (1996).
6. A. P. Alivisatos, Science (Washington, D.C.) **217,** 933 (1996).
7. J. Z. Zhang, Acc. Chem. Res. **30,** 423 (1997).
8. H. Weller, Curr. Opin. Colloid Interface Sci. **3,** 194 (1998).
9. S. V. Gaponenko, *Optical Properties of Semiconductor Nanocrystals* (Cambridge University Press, Cambridge, 1998).
10. S. A. Empedocles and M. G. Bawendi, Acc. Chem. Res. **32,** 389 (1999).
11. L. E. Brus, J. Chem. Phys. **80,** 4403 (1984).
12. L. Spanhel, M. Haase, H. Weller, and A. Henglein, J. Am. Chem. Soc. **109,** 5649 (1987).
13. K. Sooklal, L. H. Hanus, H. J. Ploehn, and C. J. Murphy, Adv. Mater. **10,** 1083 (1998).
14. J. Huang, K. Sooklal, C. J. Murphy, and H. J. Ploehn, Chem. Mater. **11,** 3595 (1999).
15. C. B. Murray, D. J. Norris, and M. G. Bawendi, J. Am. Chem. Soc. **115,** 8706 (1993).
16. Z. A. Peng and X. Peng, J. Am. Chem. Soc. **123,** 183 (2001).
17. T. Trinidade and P. O'Brien, Adv. Mater. **8,** 161 (1996).
18. T. Trinidade and P. O'Brien, J. Mater. Chem. **6,** 343 (1996).
19. M. L. Steigerwald, A. P. Alivisatos, J. M. Gibson, T. D. Harris, R. Kortan, A. Muller, A. M. Thayer, T. M. Duncan, D. C. Douglass, and L. E. Brus, J. Am. Chem. Soc. **110,** 3046 (1988).
20. N. Herron, Y. Wang, and H. Eckert, J. Am. Chem. Soc. **112,** 1322, (1990).
21. Y. Nosaka, N. Ohta, T. Fukuyama, and N. Fujii, J. Colloid Interface Sci. **155,** 23 (1993).
22. R. Kho, C. L. Torres-Marinez, and R. K. Mehra, J. Colloid Interfac. Sci. **227,** 561 (2000).
23. J. M. Whitling, G. Spreitzer, and D. W. Wright, Adv. Mater. **12,** 1377 (2000).
24. K. M. Choi and K. J. Shea, J. Phys. Chem. **98,** 3207 (1994).
25. M. P. Pileni, L. Motte, and C. Petit, Chem. Mater. **4,** 338 (1992).
26. X. K. Zhao, S. Baral, R. Rolandi, and J. H. Fendler, J. Am. Chem. Soc. **110,** 1012 (1988).
27. R. S. Urquhart, D. N. Furlong, T. Gengenbach, N. J. Geddes, and F. Grieser, Langmuir **11,** 1127 (1995).
28. N. Herron, Y. Wang, M. Eddy, G. D. Stucky, D. Cox, K. Moller, and T. Bein, J. Am. Chem. Soc. **111,** 350 (1989).
29. K. K. W. Wong and S. Mann, Adv. Mater. **8,** 928 (1996).
30. C. T. Dameron, R. N. Reese, R. K. Mehra, A. R. Kortan, P. J. Carroll, M. L. Steigerwald, L. E. Brus, and D. R. Winge, Nature (London) **338,** 596 (1989).
31. R. N. Reese, C. A. White, and D. R. Winge, Plant Physiol. **98,** 225 (1992).
32. C. T. Dameron and D. R. Winge, Inorg. Chem. **29,** 1343 (1990).
33. R. Szweda, III–V Review **13,** 14 (2000).
34. R. L. Wells and W. L. Gladfelter, J. Cluster Science **8,** 217 (1997).
35. R. L. Wells, C. G. Pitt, A. T. McPhail, A. P. Purdy, S. Shafieezad, and R. B. Hallock, Chem. Mater. **1,** 4 (1989).
36. R. L. Wells, C. G. Pitt, A. T. McPhail, A. P. Purdy, S. Shafieezad, and R. B. Hallock, Mater. Res. Soc. Symp. Proc. **131,** 45 (1989).
37. J. R. Heath, J. Phys. Chem. **100,** 7212 (1996).
38. O. Micic, B. Smith, and A. Nozik, J. Phys. Chem. B **104,** 12149 (2000).
39. Y. Cao and U. Banin, J. Am. Chem. Soc. **122,** 9693 (2000).
40. F. A. Ponce and D. P. Bour, Nature (London) **386,** 351 (1997).
41. S. Nakamura, Solid State Commun. **102,** 237 (1997).
42. J. F. Janik and R. L. Wells, Chem. Mater. **8,** 2708 (1996).
43. J. F. Janik and R. L. Wells, Inorg. Chem. **36,** 4135 (1997).
44. K. Littau, P. Szajowski, A. Muller, A. Kortan, and L. Brus, J. Phys. Chem. **97,** 1224 (1993).
45. L. Brus, P. Szajowski, W. Wilson, T. Harris, S. Schupler, and P. Citrin, J. Am. Chem. Soc. **117,** 2915 (1995).
46. W. L. Wilson, P. F. Szajowski, and L. E. Brus, Science (Washington, D.C.) **262,** 1242 (1993).
47. T. Murthy, N. Miyamoto, M. Shibo, and

J. Nishizawa, J. Cryst. Growth **33,** 1 (1976).
48. R. A. Bley and S. Kauzlarich, J. Am. Chem. Soc. **118,** 12461 (1996).
49. B. R. Taylor, S. M. Kauzlarich, H. W. H. Lee, and G. R. Delgado, Chem. Mater. **10,** 22 (1998).
50. B. R. Taylor, S. M. Kauzlarich, G. R. Delgado, and H. W. H. Lee, Chem. Mater. **11,** 2493 (1999).
51. C.-S. Yang, S. M. Kauzlarich, and Y. C. Wang, Chem. Mater. **11,** 3666 (1999).
52. C.-S. Yang, Q. Liu, S. M. Kauzlarich, and B. Phillips, Chem. Mater. **12,** 983 (2000).
53. C.-S. Yang, R. A. Bley, S. M. Kauzlarich, H. W. H. Lee, and G. R. Delgado, J. Am. Chem. Soc. **121,** 5191 (1999).
54. J. Ji, R. Senter, and J. Coffer, unpublished results.
55. A. Uhilir, Bell Syst. Tech. J. **35,** 333 (1956).
56. L. Canham, Appl. Phys. Lett. **57,** 1046 (1990).
57. M. P. Stewart and J. M. Buriak, Adv. Mater. **12,** 859 (2000).
58. H.-C. Choi and J. M. Buriak, Chem. Commun. 1669 (2000).
59. R. Cohen, L. Kronik, A. Shanzer, D. Cahen, A. Liu, Y. Rosenwaks, J. K. Lorenz, and A. B. Ellis, J. Am. Chem. Soc. **121,** 10545 (1999).
60. M. A. Hines and P. Guyot-Sionnest, J. Phys. Chem. **100,** 468 (1996).
61. X. Peng, M. C. Schalmp, A. V. Kadavanich, and A. P. Alivisatos, J. Am. Chem. Soc. **119,** 7019 (1997).
62. M. Nirmal and L. Brus, Acc. Chem. Res. **32,** 407 (1999).
63. J. Coffer, M. Johnson, L. Zhang, R. Wells, and J. Janik, Chem. Mater. **9,** 2671 (1997).
64. K. Sooklal, B. Cullum, S. M. Angel, and C. J. Murphy, J. Phys. Chem. **96,** 4551 (1996).
65. L. Levy, N. Feltin, D. Ingert, and M. P. Pileni, J. Phys. Chem. B **101,** 9153 (1997).
66. T. Nutz, U. zum Felde, and M. Haase, J. Chem. Phys. **110,** 12142 (1999).
67. H. Meyssamy, K. Riwotzki, A. Kornowski, S. Naused, and M. Haase, Adv. Mater. **11,** 840 (1999).
68. F. V. Mikulec, M. Kuno, M. Bennati, D. A. Hall, R. G. Griffin, and M. G. Bawendi, J. Am. Chem. Soc. **122,** 2532 (2000).
69. K. Riwotzki, H. Meyssamy, A. Kornowski, and M. Haase, J. Phys. Chem. B **104,** 2824 (2000).
70. P. Yang, M. K. Lu, D. Xu, D. L. Yuan, and G. J. Zhou, Chem. Phys. Lett. **336,** 76 (2001).
71. J. St. John, J. Coffer, Y. Chen, and R. Pinizzotto, J. Am. Chem. Soc. **121,** 1888 (1999).
72. J. St. John, J. Coffer, Y. Chen, and R. Pinizzotto, Appl. Phys. Lett. **77,** 1635 (2000).
73. C. Weisbuch and B. Vinter, *Quantum Semiconductor Structures: Fundamentals and Applications* (Academic Press, San Diego, 1991).
74. P. M. Petroff, A. Lorke, and A. Imamoglu, Phys. Today **54,** 46 (2001).
75. C. Livermore, C. H. Crouch, R. M. Westervelt, K. L. Campman, and A. L. Gossard, Science (Washington, D.C.) **274,** 1332 (1996).
76. D. Gammon, Nature (London) **405,** 899 (2000).
77. S. Schuppler, S. L. Friedman, M. A. Marcus, D. L. Adler, Y.-H. Xie, F. M. Ross, T. D. Harris, W. L. Brown, Y. J. Chabal, L. E. Brus, and P. H. Citrin, Phys. Rev. Lett. **72,** 2648 (1994).
78. V. Colvin, M. C. Schlamp, and A. P. Alivisatos, Nature (London) **370,** 374 (1994).
79. D. Childs, S. Malik, P. Siverns, C. Roberts, and R. Murray, Mater. Res. Soc. Symp. Proc. **571,** 267 (2000).
80. J. Faist, F. Carpasso, D. L. Sivco, C. Sirtori, A. L. Hutchinson, and A. Y. Cho, Science (Washington, D.C.) **264,** 553 (1994).
81. A. Treducucci, C. Gmachi, F. Capasso, D. L. Sivco, A. L. Hutchinson, and A. Y. Chao, Nature (London) **396,** 350 (1998).
82. N. S. Wingreen and C. A. Stafford, IEEE J. Quantum Electron. **33,** 1170 (1997).
83. V. I. Klimov, A. A. Mikhailovsky, S. Xu, A. Malko, J. A. Hollingsworth, C. A. Leatherdale, H.-J. Eisler, and M. G. Bawendi, Science (Washington, D.C.) **290,** 314 (2000).
84. L. T. Canham, in *Frontiers of Nano-Optoelectronics,* L. Pavesi and F. Buzaneva, Eds. (Kluwer Academic, Boston, 2000), pp. 85–87.
85. A. G. Cullis, L. Canham, and P. D. J. Calcott, J. Appl. Phys. **82,** 909 (1997).
86. L. Pavesi, L. Dal Negro, C. Massoleni, G. Franzo, and F. Priolo, Nature (London) **408,** 440 (2000).
87. Y. Kanemitsu and S. Okamoto, Solid State Commun. **103,** 573 (1997).
88. Y. Kanemitsu and S. Okamoto, Phys. Rev. B: **58,** 9652 (1998).
89. L. Canham, Nature (London) **408,** 411 (2000).
90. H. Lopez and P. Fauchet, Appl. Phys. Lett. **75,** 3989 (1999).
91. H. Lopez and P. Fauchet, Appl. Phys. Lett. **77,** 3704 (2000).
92. J. D. Joannopoulos, R. D. Meade, and J. N. Winn, *Photonic Crystals: Molding the Flow of Light* (Princeton University Press, Princeton, NJ, 1995).
93. W. U. Huynh, X. Peng, and A. P. Alivisatos, Adv. Mater. **11,** 923 (1999).
94. M. Bruchez, Jr., M. Moronne, P. Gin, S. Weiss, and A. P. Alivisatos, Science (Washington, D.C.) **281,** 2013 (1998).
95. W. C. W. Chan and S. Nie, Science (London) **281,** 2016 (1998).
96. H. Mattoussi, J. M. Mauro, E. R. Goldman, G. P. Anderson, V. C. Sundar, F. V. Mikulec, and M. G. Bawendi, J. Am. Chem. Soc. **122,** 12142 (2000).
97. S. Pathak, S.-K. Choi, N. Arnheim, and M. E. Thompson, J. Am. Chem. Soc. **123,** 4103 (2001).
98. M. Y. Han, X. H. Gao, J. Z. Su, and S. Nie, Nature Biotechnology **19,** 631 (2001).
99. D. Gerion, F. Pinaud, S. C. Williams, W. J. Parak, D. Zanchet, S. Weiss, and A. P. Alivisatos, J. Phys. Chem. B **105,** 8861 (2001).
100. J. Lee, V. C. Sundar, J. R. Heine, M. G. Bawendi, and K. F. Jensen, Adv. Mater. **12,** 1311 (2000).
101. R. Mahtab, J. P. Rogers, and C. J. Murphy, J. Am. Chem. Soc. **117,** 9099 (1995).
102. R. Mahtab, J. P. Rogers, C. P. Singleton, and C. J. Murphy, J. Am. Chem. Soc. **118,** 7028 (1996).
103. R. Mahtab, H. H. Harden, and C. J. Murphy, J. Am. Chem. Soc. **122,** 14 (2000).
104. J. R. Lakowicz, I. Grycynski, Z. Grycynski, K. Nowaczyk, and C. J. Murphy, Anal. Biochem. **280,** 128 (2000).
105. R. Mahtab and C. J. Murphy, Proc. SPIE-Int. Soc. Opt. Eng. **3924,** 10 (2000).
106. L. Gearheart, K. Caswell, and C. J. Murphy, J. Biomed. Optics **6,** 111 (2001).
107. J. T. Hu, L. S. Li, W. D. Yang, L. Manna, L. W. Wang, and A. P. Alivisatos, Science (Washington, D.C.) **292,** 2060 (2001).
108. M. H. Huang, S. Mao, H. Feick, H. Q. Yan, Y. Y. Wu, H. Kind, E. Weber, R. Russo, and P. D. Yang, Science (Washington, D.C.) **292,** 1897 (2001).
109. C. J. Murphy, Adv. Photochem. **26,** 145 (2001).